VOL. 13, NO. 21, NOVEMBER 2018 ISSN 1819-6608
ARPN Journal of Engineering and Applied Sciences

www.arpnjournals.com

COMPARATIVE STUDY OF TURBULENT INCOMPRESSIBLE FLOW PAST NACA AIRFOILS

Aslam Abdullah, Amirul Aizad Roslan and Zamri Omar
Department of Aeronautical Engineering, Faculty of Mechanical and Manufacturing Engineering,
Universiti Tun Hussein Onn Malaysia, Parit Raja, Batu Pahat, Johor, Malaysia
E-Mail: aslam@uthm.edu.my

ABSTRACT

The flow past the airfoils is continuously investigated in various experimental and computational aerodynamic perspectives. In this paper, a comparative study on the aerodynamic characteristics of the turbulent incompressible flow past four NACA airfoils is emphasized. Particularly, we classify these characteristics based on the basic geometries, namely symmetric and asymmetric airfoils, as well as trailing edge angles. The results confirm the general aerodynamic theory and include finding on the effect of sharp trailing edge, which complement the available airfoil datasets for improving their designs and as reference cases.

Keywords: NACA airfoils, symmetric airfoils, unsymmetric airfoils, sharp trailing edge, turbulent incompressible flow.

1. INTRODUCTION

Among early important researches that take turbulent incompressible flow past an airfoil into account is [1] where the numerical experiment was done in investigating the flow properties. This type of research has been going on since then. In particular, works done by [2] and [3], for instance, indicate the necessity of continuous numerical investigation of airfoil aerodynamics. This long tradition can be explained, by the interests in airfoils design [4], high lift device [5], ground effects [6]-[7], and flow separation control [8]-[11].

This study aims not only to contribute to the turbulent incompressible aerodynamic data for airfoils of interest in order to complement those for compressible flow, but also compare the outputs.

The Mach number M<0.3 is considered, where the compressibility effect is assumed to be negligible. Thus, it does not need to be taken into consideration in the calculation of aerodynamic properties. Such incompressible flows are classified into subsonic flows since M<1 [12].

The paper compares the aerodynamic performance of the airfoils in turbulent incompressible subsonic flow. A steady-state Reynolds-averaged Navier-Stokes (RANS) investigation was performed using the commercial CFD code ANSYS. The wing cross-sections were divided into symmetrical or un-cambered (i.e. NACA 0015 and NACA 0018) and asymmetrical or cambered airfoils (i.e. NACA 2412 and NACA 63-415). The characteristics of flow over four airfoils of interest were evaluated. The airfoils form the cross sections of passenger airplanes shown in Table I.

The comparison for both types of airfoil should fall within the scope of the fundamental airfoil theories such as in the case of the lift and drag production versus angle of attack α as well as the critical or stall angle of attack α_c beyond which the lift degrades [13].

Table-1. Airfoils of interest and their corresponding passenger airplanes.

Airfoil series	Passenger airplane
NACA 0015	Lockheed L-1649A Starliner
NACA 0018	Boeing 314 Clipper
NACA 2412	Cessna 170
NACA 63-415	Convair CV-240

2. GOVERNING EQUATIONS AND MODELLING ASSUMPTIONS

In the calculation of incompressible, steady, 2-D turbulent flow around the airfoil, a finite volume numerical method based on solving RANS equations was used:

$$\rho\left(u_1\frac{\partial u_1}{\partial x_1}+u_2\frac{\partial u_1}{\partial x_2}\right)+\frac{\partial P}{\partial x_1}+\rho\left(\frac{\partial <u_1'u_1'>}{\partial x_1}+\frac{\partial <u_1'u_2'>}{\partial x_2}\right)=F_1+\mu\left(\frac{\partial^2 u_1}{\partial x_1^2}+\frac{\partial^2 u_1}{\partial x_2^2}\right), \quad (1)$$

and

$$\rho\left(u_1\frac{\partial u_2}{\partial x_1}+u_2\frac{\partial u_2}{\partial x_2}\right)+\frac{\partial P}{\partial x_2}+\rho\left(\frac{\partial <u_1'u_2'>}{\partial x_1}+\frac{\partial <u_2'u_2'>}{\partial x_2}\right),=F_2+\mu\left(\frac{\partial^2 u_2}{\partial x_1^2}+\frac{\partial^2 u_2}{\partial x_2^2}\right), \quad (2)$$

where u_1, u_2 are time-averaged velocity vectors, u_1', u_2' are fluctuating velocity vectors, P is the pressure, F_1, F_2 are body forces, and μ is the dynamic viscosity. The continuity equation,

$$\frac{\partial u_1}{\partial x_1} + \frac{\partial u_2}{\partial x_2} = 0 \quad (3)$$

must be satisfied by (1) and (2).

The Reynolds averaging in the derivation of (1) and (2) results in the Reynolds or turbulence stresses which need to be mathematically modelled. In particular, the Spalart-Allmaras turbulence model which gives a general description of turbulence by means of single transport equation was used to ensure the closure of the equations. The reason why this model consists of only one equation is that it is grounded on the assumption of zero turbulence kinetic energy. Further explanation on the selection of the turbulence model is given in [14].

The method is applied with second-order upwind discretization schemes. The algorithm called SIMPLE is employed for the velocity-pressure coupling. The airfoil velocity and the Reynolds number are 5.4 m/s and 3.6 x 10^5, respectively. The Mach number of flow is 0.02. Thus, the compressibility effects could be neglected. The density as well as dynamic viscosity are set to be those at sea level (i.e. 1.225 kg/m^3 and 1.8375 x 10^{-5} kg/ms, respectively). It is necessary to vary the angle of attack in the investigation.

3. GEOMETRY, GRID AND DOMAIN

The flow of interest is that over the NACA 0015, NACA 0018, NACA 2412, and NACA 63-415 airfoils. Among these airfoils, NACA 0015 and NACA 0018 are labelled here as symmetric airfoils based on their relative geometries given in Figure-1. All airfoil models are in unbounded flow. The grid used for calculations is given in Figure-2.

For discretization of the computational domain, an unstructured type of grid with quad elements was selected. Inlet and outlet boundary conditions were specified on the outer sides of computational domain with necessary turbulence and flow parameters. The argument that all solid surfaces are practically rough on a microscopic scale supports the idea of no-slip boundary condition. It is evidence that the energy lost through viscous dissipation as a fluid passes over and around the irregularities is sufficient to ensure that it is effectively brought to rest [15]. Therefore the velocity of the air at the surface of the airfoil was set to zero.

4. RESULTS OF CALCULATIONS

The velocity distribution, lift and drag profiles are the focus of discussion. As shown in Figure-3, the velocity fields of interest around the airfoils are those for $\alpha = \alpha_o = 0$ and α_c. The airfoils are in unbounded flow.

A moment after α_c is reached, the induced velocity differences are higher, which result in the increase of lift, and directly influence lift-to-drag ratio *L*/*D*. The stagnation-points shift from the leading edges at α_o to the lower sides of the airfoils at α_c. The field contours in Figures 3(a)-3(b) at α_o are symmetrical about the chord lines as expected for un-cambered airfoil geometries (i.e. NACA 0015 and NACA 0018), in comparison to those in Figure-3(c)-3(d).

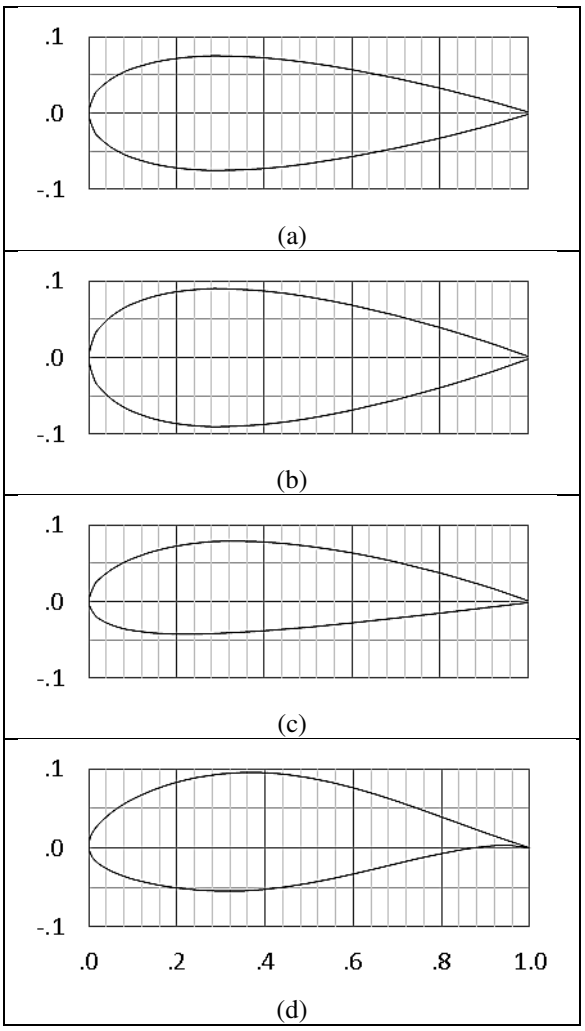

Figure 1. Geometry of airfoils (a) NACA 0015(b) NACA 0018 (c) NACA 2412 (d) NACA 63-415.

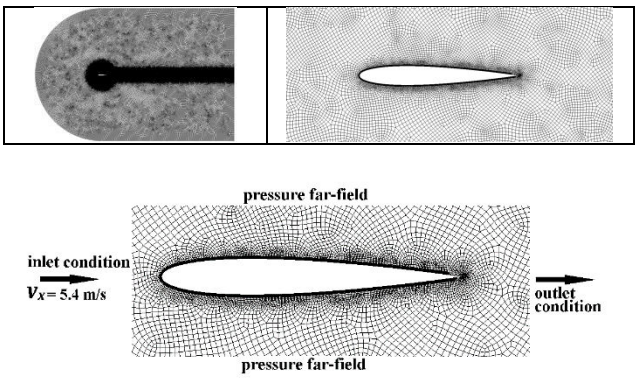

Figure-2. Grid applied for airfoil moving in unbounded flow.

The early signs of flow separation emerge at α_c which are yet to be fully developed. It is not clear which of the flow is most attached in all cases, unlike in the case of high Reynolds number compressible flow [4]. Note, however, that the flow past NACA 2412 separation region is the largest. More detailed study is necessary to relate the onset of flow separation to α_c.

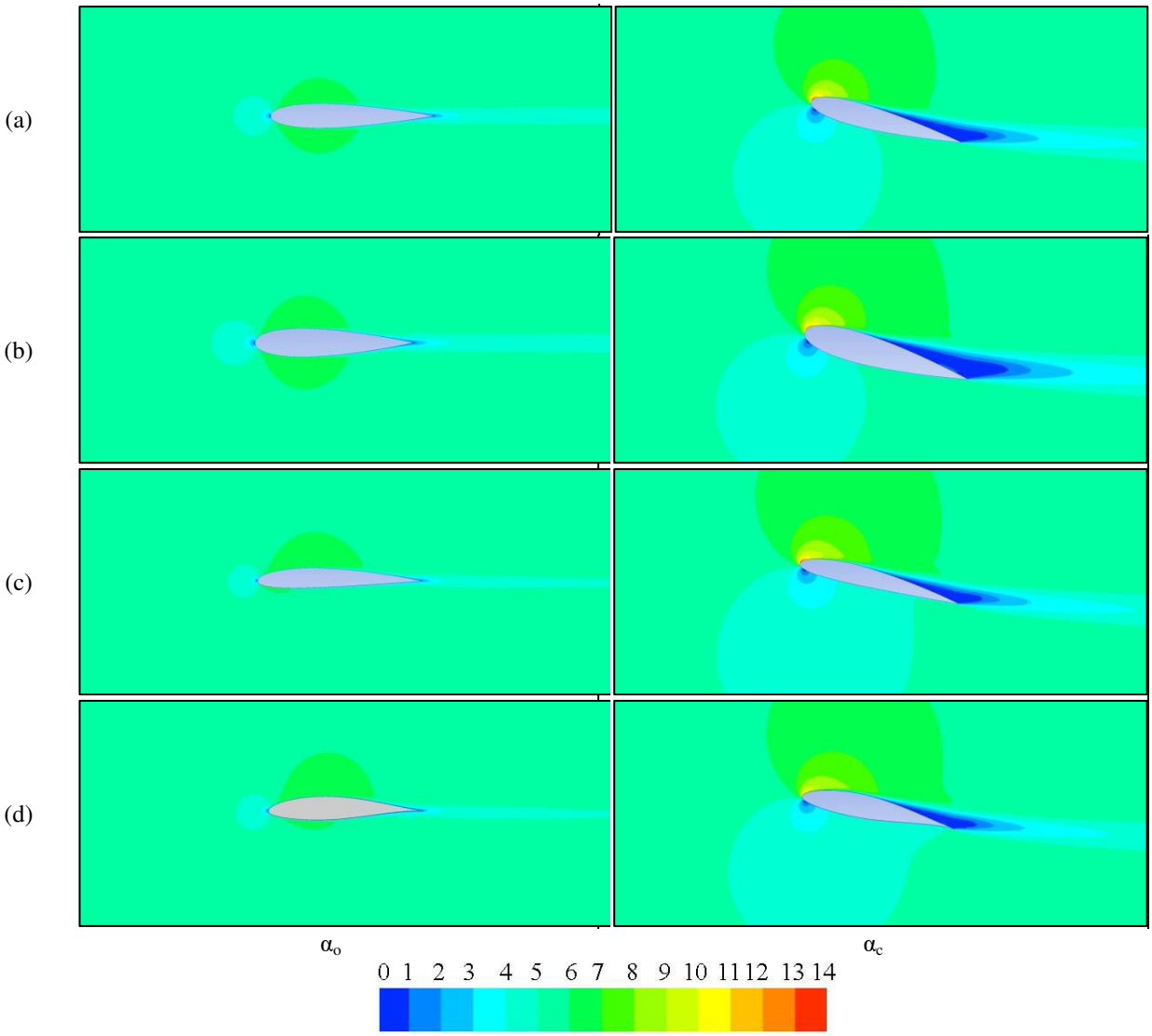

Figure-3. Velocity contour in m/s at α_o and α_c (a) NACA 0015 (b) NACA 0018 (c) NACA 2412 (d) NACA 63-415.

Higher lift and earlier stall can be seen for both cambered NACA 2412 and NACA 63-415 airfoils, while greater α_c are found for both symmetric NACA 0015 and NACA 0018 airfoils as in Figure-4.

The airfoil NACA 63-415 with the relatively smallest trailing edge angle needs further attention. The flow produces the highest lift prior to stall, and the highest drag for $\alpha > 6$. The flows past three other airfoils produce relatively similar C_d values as can be seen in Figure-5.

5. FINAL REMARKS

The comparative aerodynamic properties of four airfoils, namely NACA 0015, NACA 0018, NACA 2412 and NACA 63-415, have been studied. The main outcomes can be summarized as follows:

At stall angle of attack, the pressure side of the airfoil prevents the incoming air to flow smoothly through the top surface of the airfoil, where the flow separation begins to take place.

At a given angle of attack, the pressure difference across the asymmetrical airfoils (i.e. NACA 2412 and NACA 63-415) results in higher lift than that across the symmetrical air foils (i.e. NACA 0015 and NACA 0018).The former, however, experience rapid drop of lift as stall angle of attack is reached.

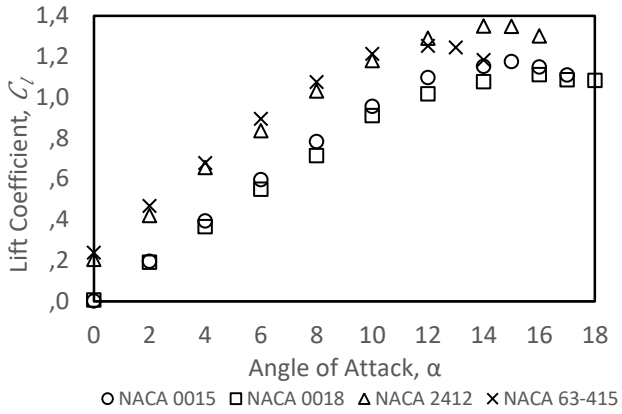

Figure-4. The lift coefficient C_l profiles.

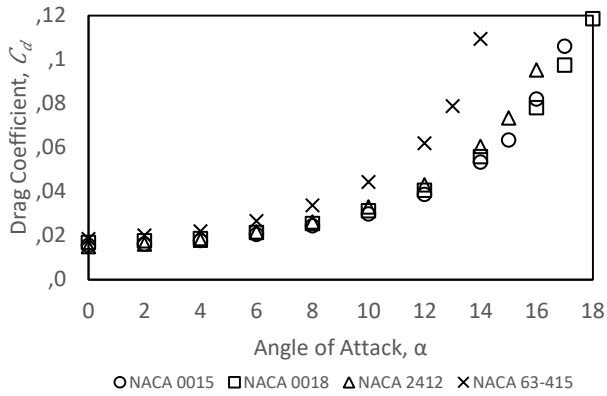

Figure-5. The drag coefficient C_d profiles.

In general, the airfoil NACA 63-415 experiences the highest drag mainly due to the presence of small/sharp trailing edge angle.

ACKNOWLEDGEMENT

The author would like to thank Universiti Tun Hussein Onn Malaysia (UTHM) and Ministry of Higher Education of Malaysia (MoHE) for the research facilities.

REFERENCES

[1] Rhie W. L. and Chow C. M. 1983. Numerical study of the turbulent flow past an airfoil with trailing edge separation. AIAA J. 11: 1525-1532.

[2] Petinrin M. and Onoja V. 2017. Computational study of aerodynamic flow over NACA 4412 airfoil. Br. J. Appl. Sci. Technol. 21: 1-11.

[3] Khan T. A., Li W., Zhang J. and Shih T. I. P.2017. Local vibrations and lift performance of low Reynolds number airfoil. Psychol. Learn. Motiv. - Adv. Res. Theory. 67: 79-90.

[4] Abdullah A., Jafri M. N. S. M. and Zulkafli M. F. 2017. Numerical study of military airfoils design for compressible flow. ARPN J. Eng. Appl. Sci. 12.

[5] Khoshlessan M. and Karimian S. M. H. 2017.Detailed numerical study on the aerodynamic behavior of a gurney flapped airfoil in the ultra-low Reynolds regime. J. Aerosp. Technol. Manag. 9: 194-208.

[6] Abdullah A., Yazi M. N., Ghafir M. F. A., Mohd S. and Rahim M. Z. 2017. Ground proximity effect on the flow over NACA 4412 multi-element airfoil in clean configuration. J. Phys. Conf. Ser. 914.

[7] Abdullah A., Kamsani M. A. and Abdullah K. 2017. Effect of ground proximity on the flow over STOL CH750 multi-element airfoil. IOP Conf. Ser. Mater. Sci. Eng. 243.

[8] Munday P. M. and Taira K. 2017. Effects of wall-normal and angular momentum injections in airfoil separation control. 1-20.

[9] Mashud M., Shaha S. and Haque E. 2017. Enhancement of lift to drag ratio of anairfoil by using continuous normal suction. ICMERE2017. 2017: 18-20.

[10] Nottingham T., User N. E., Pasquale L. and Zanchetta P. 2018. Output feedback control of flow separation over an aerofoil using plasma actuators. International Journal of Numerical Analysis and Modeling. 5105: 1705-5105 (In Press).

[11] Nottingham T. and User N. E. 2017. Robust feedback control of flow separation using plasma actuators.

[12] Rathakrishnan E. 2013. Theoretical aerodynamics. Singapore: John Wiley and Sons Singapore Pte. Ltd.

[13] Abbott I. H. and Doenhoff A. 1959. Theory of wing sections. New York: Dover Publications Inc.

[14] Abdullah A. 2012. Quantifying guidelines and criteria for using turbulence models in complex flows. PhD Thesis.

[15] Richardson S. 1973. On the no-slip boundary condition. J. Fluid Mech. 59: 707-719.